BEILSTEIN JOURNAL OF NANOTECHNOLOGY

Closing the gap in antibacterial nanomaterials: why black phosphorus matters

Paniz Olapour and Dominikus Heift*

Review

Open Access

Address:
School of Life Sciences, Pharmacy and Chemistry, Kingston University, Penrhyn Road, Kingston-upon-Thames KT1 2EE, UK

Email:
Dominikus Heift* - d.heift@kingston.ac.uk

* Corresponding author

Keywords:
antibacterial 2D materials; antimicrobial resistance; black phosphorus; comparative antibacterial efficacy; nanoknife effect; photodynamic therapy; photothermal therapy; wound infection control

Beilstein J. Nanotechnol. **2026,** *17,* 1682–1698.
https://doi.org/10.3762/bjnano.17.116

Received: 09 July 2026
Accepted: 05 November 2026
Published: 27 November 2026

Associate Editor: A. Salvati

© 2026 Olapour and Heift; licensee Beilstein-Institut.
License and terms: see end of document.

Abstract

The rapid emergence of antimicrobial resistance highlights the urgent need for antibacterial strategies beyond conventional antibiotics. Two-dimensional (2D) nanocomposites have attracted considerable interest as alternative antimicrobial materials; however, many of them are constrained by poor biodegradability, long-term toxicity, and limited control over targeted reactivity. This article critically evaluates black phosphorus (BP), a biodegradable 2D material for antibacterial applications. Systematically we compare its physicochemical properties and antibacterial performance with other nanomaterials, including graphene oxide, metal nanoparticles, and transition metal dichalcogenides. BP's distinct advantage arises from its controlled degradation into nontoxic phosphate ions, effectively overcoming the bio-persistence concerns associated with many nanomaterials. Importantly, BP exhibits multifaceted antibacterial activity through complementary mechanisms, including contact-mediated membrane disruption (nanoknife effect), photodynamic activity driven by reactive oxygen species generation, and photothermal activity under near-infrared irradiation. Surface passivation by chemical modification and integration of BP into polymers for metal-based composites can improve the stability of BP and target antibacterial efficacy in certain biological environments (e.g., different pH conditions).

Review

Introduction

Bacterial infections remain a major global health challenge, with antimicrobial resistance representing one of the most urgent threats to public health worldwide [1-5]. Prolonged and widespread antibiotic misuse has accelerated the emergence of multidrug-resistant pathogens, including methicillin-resistant bacteria like *Staphylococcus aureus* [1] and *Acinetobacter baumannii*, which is classified by the World Health Organization as a critical-priority bacterium [6]. Collectively, pathogens within the "ESKAPE group" (*Enterococcus faecium*, *Staphylococcus aureus*, *Klebsiella pneumoniae*, *Acinetobacter baumannii*, *Pseudomonas aeruginosa*, and *Enterobacter* species) exhibit advanced resistance mechanisms that limit the

effectiveness of current therapies and contribute to severe clinical conditions such as septicaemia and delayed wound healing [5].

Drug-resistant infections are estimated to cause approximately 700,000 deaths annually and are projected to reach 10 million per year by 2050, with associated economic losses exceeding $100 trillion [2,5]. The slow pace of antibiotic development and the rapid increase of resistance highlight the urgent need for alternative antibacterial strategies beyond conventional medication [2,3,7,8].

In this context, nanomaterial-based antibacterial formulations have attracted increasing attention due to their ability to impose different antimicrobial actions that are less prone to resistance development. Among these, two-dimensional (2D) nanomaterials are of particular interest because their ultrathin shapes provide large surface areas, sharp edges capable of membrane disruption, and sometimes also tuneable photothermal properties [8-10]. Representative antibacterial 2D systems include graphene-based materials [8,11], MXenes [9,12,13], transition-metal dichalcogenides such as MoS_2 [10,14,15], hexagonal boron nitride (h-BN) [16,17] and metal or metal oxide nanoparticles including silver, gold, copper, and zinc oxide [18-25]. These materials typically can cause antibacterial activity through contact-mediated membrane damage, reactive oxygen species (ROS) generation, surface-charge-driven cell binding, or photothermal heating under near-infrared (NIR) irradiation. [8-14,18,22-24,26,27]. However, their clinical application is frequently hindered by fundamental limitations such as poor biodegradability, long-term biosafety concerns, aggregation and loss of activity in physiological environments, or limited selectivity between bacterial and mammalian cells [8-12,14,18,20,22-25,28-30]. These challenges have driven the development of antibacterial nanomaterials that retain strong activity while exhibiting improved biodegradability, tuneable reactivity, and safe in vivo performance [8-10,12-14,23].

Among the 2D materials, black phosphorus (BP) has attracted significant interest as an antibacterial nanomaterial [31]; thus, it is instructive to briefly consider the historical discovery of various phosphorus allotropes. White phosphorus (P_4) was first isolated in 1669 by the German alchemist Hennig Brand through the reduction of phosphate salts, one of the first elements obtained by chemical methods [32]. Subsequent research revealed a diverse family of phosphorus allotropes with distinct properties, including red, violet (Hittorf's), black, fibrous, and more recently blue and green phosphorus [32-37]. Among all allotropes, BP is by far the most thermodynamically stable form of the element [38]. Although BP was already synthesized in 1914 via high-pressure, high-temperature conversion of white phosphorus [5,33], it remained largely unexplored for decades, primarily due to the challenging synthetic access.

Structurally, BP consists of puckered layers of sp^3-hybridized phosphorus atoms, each bearing a lone pair that offers potential for chemical functionalization. These honeycomb-structured layers are held together by van der Waals forces [39]. Unlike graphene, BP is a semiconductor, with a layer-dependent bandgap ranging from approximately 0.3 eV in the bulk to 1.5–2 eV in monolayer phosphorene [33,39]. This tuneable bandgap enables BP's efficient photothermal activity and ROS generation under light exposure, both of which are central to its antibacterial activity (vide infra) [39]. In addition to its optical responsiveness, BP exhibits several other characteristics that are particularly advantageous for antibacterial applications. For example, its puckered lattice gives rise to strong in-plane anisotropy (distinct armchair and zigzag crystallographic directions), which results in direction-dependent electronic and chemical reactivity and can enhance interactions with bacterial membranes (see Figure 1 for a schematic illustration) [5,38,40,41].

Exfoliated BP nanosheets possess a large surface area and sharp edges that can physically disrupt bacterial cell membranes through a contact-based "nanoknife" mechanism [2,43]. The presence of surface-exposed lone-pair electrons facilitates interactions with biological molecules, contributing to antibacterial efficacy [5,38,39]. Importantly, BP undergoes controlled degradation into nontoxic phosphate ions under physiological conditions, a key advantage compared to many non-degradable 2D nanomaterials [44]. Together, these properties distinguish BP as a biodegradable, antibacterial material capable of physical cell wall disruption, oxidative stress induction, and photothermal effects. Building on these advantages, this review critically evaluates BP as an antibacterial nanomaterial in comparison with alternative 2D composites. In contrast to other reviews on this topic, this article not only discusses recent developments in the field but compares BP against alternative nanomaterials while critically examining the balance between its biodegradability, stability, and antibacterial efficacy, highlighting both its potential advantages and the challenges associated with its biomedical applications.

Synthesis of black phosphorus

BP nanosheets can be synthesized using several approaches, selected according to the intended application and required material quality [45,46]. Classically, BP is produced from red phosphorus via a chemical vapour transport (CVT) process using SnI_4 as a catalyst. While this method yields high-purity BP with a well-ordered layered structure, it is highly expensive and limited to small-scale production (typically up to 1 g)

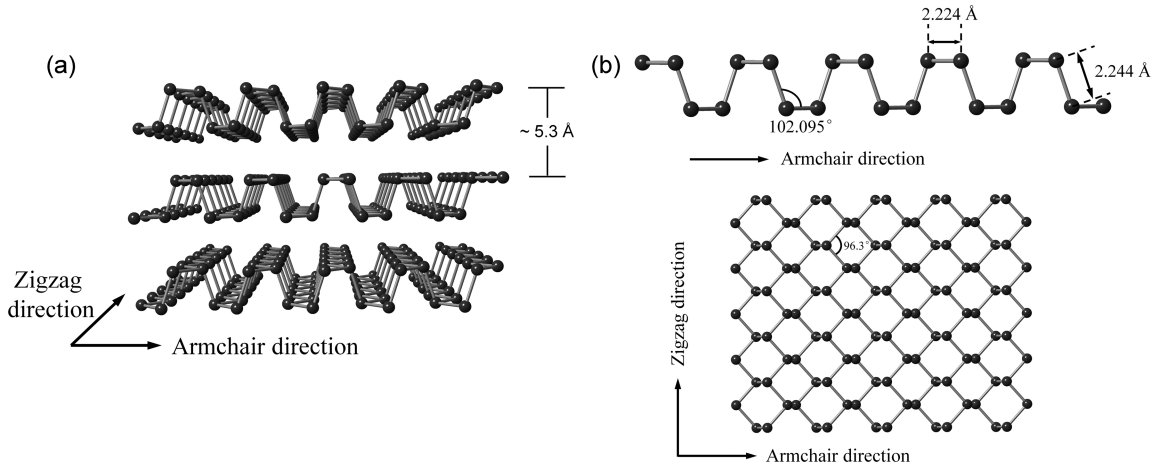

Figure 1: Crystal structure of black phosphorus showing the two main crystallographic directions: (a) zigzag (ZZ, perpendicular to the puckering) and armchair (AC, parallel to the puckering), and (b) selected bond angles, bond lengths and top view of the BP structure. Reproduced with permission from [42]. Copyright © The Royal Society of Chemistry 2015. This content is not subject to CC BY 4.0.

[2,33,45,47]. In contrast to CVT processes, mechanochemical synthesis enables scalable production of BP nanomaterials via direct conversion of red phosphorus to BP in a high-energy ball mill (HEBM), exploiting kinetic energy [48,49]. Importantly, this is a solvent-free, safe process reducing energy input and hazardous waste. This method allows for BP production on a multigram scale; however, the produced BP is more amorphous in nature. High-energy ball-milling also allows for in situ functionalization of the BP surface, yielding, for example, polymer-stabilized BP nanohybrids with improved aqueous stability and biocompatibility [50]. More recently, solvothermal methods in ethylenediamine have been developed that allow the conversion of red phosphorus to BP on a larger scale [51]. However, BP materials produced via solvothermal methods often contain residual traces of hazardous ethylenediamine. Therefore, for biomedical applications, HEBM and CVT methods are more commonly employed for BP synthesis.

Sustainability and biocompatibility of black phosphorus

To assess the suitability of BP for antimicrobial applications, its synthesis strategies and sustainability profile are here evaluated in comparison with carbon-based and other 2D nanomaterials (see Table 1). In the biomedical context, sustainability can be broadly assessed by four criteria, namely, biodegradability, toxicity of degradation products, environmental impact of synthesis routes, and resource renewability [2,52]. BP exhibits a clear advantage in biodegradability as it degrades into nontoxic phosphate ions in aqueous environments, particularly under light and oxygen exposure [52,53]. In contrast, graphene oxide (GO) can persist in biological systems and has been associated with long-term accumulation and oxidative stress [54]. Transition metal dichalcogenides (TMDs), despite their strong antibacterial performance, are generally non-degradable and may present cytotoxicity concerns [55]. MXenes offer high tunability and antibacterial efficacy; however, metal ion toxicity and synthesis complexity raise sustainability concerns [55,56]. Hexagonal boron nitride (h-BN) exhibits high chemical stability and biosafety but shows limited antimicrobial activity unless combined with additional agents [57]. Similarly, inorganic nanoparticles such as zinc oxide, silver, and copper show strong antibacterial effects and efficient ROS generation; yet, their non-biodegradability, metal ion leaching, and dose-dependent cytotoxicity raise environmental and health concerns [58].

While GO is widely studied for antimicrobial applications, its oxidative stress potential and “environmentally intensive” synthesis routes remain key limitations [54]. Compared to other carbon-based nanomaterials the synthesis of GO (Hummers’ method) relies on harsh oxidizing conditions [54]. Although graphite precursors are inexpensive, the extensive purification steps required for biomedical-grade GO production introduce substantial costs, including high water and energy consumption for washing, neutralization, and impurity removal [85].

In contrast, the synthesis of BP, particularly via HEBM, avoids strong acids and oxidizers, aligning more closely with green chemistry principles [52]. Even the more energy-intensive CVT synthesis of BP can be considered as “environmentally cleaner” than the production of high-purity GO [2,54]. Thus, despite current challenges related to scalability and stability, BP exhibits a sustainability advantage over many competing nanomaterials, including GO (Table 2) [2,45,52,54].

Table 1: Material properties of BP in comparison to other nanomaterials used in biomedicine.

Features	
Biocompatibility and biodegradability	
BP	biodegradable and variable biocompatibility [52,53]
MXenes	surface- and dose-dependent biocompatibility. Variable oxidative degradation [59]
TMDs	variable biocompatibility, composition-dependent degradation [2,55,60]
H-BN	neutrophil-mediated biodegradation, increased cytotoxicity after degradation [61]
ZnO	dose-dependent cytotoxicity, pH-dependent chemical dissolution [58,62]
Ag and Cu NPs	size- and dose-dependent cytotoxicity, partial dissolution [58,63,64]
GO	size- and dose-dependent cytotoxicity, enzymatic biodegradation [54,65]
Stability under ambient conditions	
BP	prone to oxidation [66,67]
MXenes	size-dependent oxidation susceptibility [68]
TMDs	S-based relatively air-stable, Te-based air-sensitive [69]
H-BN	air-stable [70]
ZnO	bulk stable, humidity- and CO_2-sensitive surface [60]
Ag and Cu NPs	relatively stable, depending on particle size and storage conditions [58,71,72]
GO	gradual structural changes during ambient ageing [73]
Sustainability	
BP	excellent biodegradability. Reduced bioaccumulation potential [52,53]
MXenes	concern over persistence [55,56]
TMDs	composition-dependent persistence and clearance concerns [55]
H-BN	degradation-associated cytotoxicity concerns [61]
ZnO	potential aquatic ecotoxicity [62,74]
Ag and Cu NPs	potential aquatic and microbial ecotoxicity [58]
GO	environmental persistence and ecotoxicity concerns [54]
Toxic byproducts	
BP	non-toxic phosphate species [52,53]
MXenes	metal ion leaching [55,56]
TMDs	metal oxide species (toxicity varies) [55]
H-BN	non-cytotoxic borate/nitrate, cytotoxic residual h-BN fragments [57,61]
ZnO	metal ion leaching [58]
Ag and Cu NPs	condition-dependent metal ion leaching [58]
GO	enzymatically degraded GO: no observed cytotoxicity [54,75]
Cost and availability	
BP	costly BP from chemical vapour transport methods; low-cost, amorphous, mechanochemically produced BP [49,76]
MXenes	relatively low synthesis cost [77,78]
TMDs	low-cost, scalable synthesis of MoS_2 and WS_2 [79]
H-BN	cost-efficient synthesis [80,81]
ZnO	cost-effective synthesis [82]
Ag and Cu NPs	both commercially available, Cu generally less costly than Ag [83,84]
GO	cost-effective, graphite-based synthesis [54,65,85]

Table 2: Viability of BP compared to GO.

Methods	Cost	Sustainability	Scalability	Purity	Drawbacks
BP produced by HEBM	relatively low (vs CVT)	solvent-free, avoids hazardous mineralizers	multigram-scale production feasable	can contain traces of red phosphorus if milling time is too short	amorphous material
BP produced by CVT	relatively high (vs HEBM)	avoids strong oxidants, energy-intensive	small-scale production (typically ≤1 g)	high purity, BP crystals with layered structure	costly, small-scale production
GO produced by Hammer's method	high reagent consumption and purification costs	use of strong acids and oxidants, hazardous waste generation	commercially established, limited by reagent consumption and processing time	high purity achievable with thorough washing	use of hazardous acids and oxidants

Degradation and stabilization of black phosphorus

BP exhibits limited stability under physiological conditions, which remains a key barrier for its translation into clinical applications. This instability originates from its high surface reactivity, arising from its large surface area. Together, the puckered lattice geometry and the exposed lone-pair electrons on each phosphorus atoms promote susceptibility to oxidative degradation [66]. Upon exposure to oxygen, moisture, and light, BP undergoes oxidation to form various phosphorus oxide species (PO_x^{3-}, x = 2, 3, or 4). Although these degradation products are biocompatible, their formation results in a progressive degradation of the BP structure [66,67,86]. The BP degradation typically follows a sigmoidal profile, beginning with a slow induction phase, followed by accelerated oxidation of the BP lattice. The degradation kinetics are strongly influenced by environmental factors, including oxygen concentration, humidity, light intensity, temperature, and thickness of the BP flakes. Thicker BP flakes exhibit enhanced stability, persisting for up to two weeks under ambient conditions, whereas few-layer BP degrades within hours or days [39]. Photo-oxidation is widely recognized as the dominant degradation pathway of BP, which requires the simultaneous presence of light, oxygen, and water. Early studies by Favron et al. revealed the role of photo-induced oxidation [87], while Castellanos-Gomez et al. demonstrated that the hydrophilicity of the BP surface facilitates moisture-assisted degradation [88]. Importantly, recent work indicates that water does not directly participate in the oxidation reaction; however, it accelerates degradation by enhancing oxygen diffusion to the BP surface and stabilizing reactive oxygen species [89]. Although the instability of BP limits its long-term functionality, controlled degradation can be advantageous in specific biomedical contexts, such as wound healing, where phosphate ion release contributes to antimicrobial activity and tissue regeneration.

For applications requiring prolonged activity, however, effective stabilization strategies of the BP structure are essential [39,66]. Most chemical modification methods exploit the lone pairs on the phosphorus atoms. Covalent bonding of amines, thiols, aryl diazonium salts, or carbenes to the P centres results in the formation of stable P–N, P–S, P–C, or P=C bonds that inhibit oxidation and allow for controlled doping of BP with heteroatoms [39,67,90,91]. Also, doping with main group elements (e.g., tellurium) has been shown to enhance the stability of the BP structure by suppressing reactive oxygen species generation [2,66,92]. Besides covalent chemical modifications, surface passivation and encapsulation are widely used to improve BP stability by limiting exposure to oxidative environments [2,39]. Inorganic coatings such as Al_2O_3 and SiO_2, deposited via atomic layer deposition, can preserve the BP structure over extended periods [2,93]. Even multilayer encapsulation that combines inorganic barriers with hydrophobic coatings has been achieved [90]; however, the improved stability must be balanced with sustaining surface reactivity of the BP material.

In particular polymer-based encapsulation (e.g., with polydopamine [93] or polyethylene glycol) has been extensively employed to reduce moisture and oxygen exposure of BP nanosheets [2,66,67]. Encapsulation of BP nanosheets in polymers enhances their stability and offers the potential of therapeutic delivery. For example, incorporation into hydrogels facilitates drug delivery and photothermal therapy while promoting wound healing. Additionally, embedding BP into three-dimensional printed scaffolds supports cell proliferation and osteogenesis [67,94].

The stabilization of BP nanosheets can also be achieved through non-covalent edge functionalization of the BP nanosheets with hydrophobic molecules, for example with C_{60} (mechanochemical milling process), by addition of π-conjugated molecules (such as perylene bisimide) or through coordination of metal precursors (e.g., titanium complexes and lanthanide sulfonates) [2,66,92,95]. Encapsulation of BP with other 2D materials such as graphene or h-BN likewise preserves the structural integrity by forming physical diffusion barriers [86,90]. Importantly, 2D

encapsulation may modify the optical responsiveness and charge-transfer behaviour of BP, which can influence photothermal and ROS-mediated antibacterial functions [90]. Despite the necessity of stabilization, maintaining BP's biodegradability remains important for biomedical applications since controlled degradation ensures safe elimination of the materials from the patients after the treatment. Therefore, stabilization strategies must balance extending BP's lifespan during therapeutic delivery with preserving its capacity for biodegradation and clearance.

Antibacterial reactivity of black phosphorus

BP nanomaterials (BPNs) exhibit antimicrobial activity through combined chemical and physical mechanisms, making them promising candidates for treating bacterial infections, including drug-resistant strains [2,5]. A crucial advantage of BP is its targeted reactivity toward bacterial cells, which arises from selective interactions between the nanomaterial and cells, while maintaining relatively low cytotoxicity toward mammalian tissues [2,39]. Noteworthy, reported BP biocompatibility varies across studies and appears to depend strongly on material characteristics and exposure conditions. While several studies have reported low cytotoxicity at specific concentrations, increased mammalian-cell toxicity has also been observed at higher concentrations and with differences in BP size and structure. Therefore, the biocompatibility of BP should not be considered an intrinsic or uniform property; instead, it is size-, dose-, and formulation-dependent. The high surface area and sharp edges of BP nanosheets enable contact-dependent physical disruption of bacterial membranes, resulting in loss of membrane integrity [2,5]. This effect is more pronounced in bacterial cells due to their membrane structure and composition. Bacterial membranes are enriched with lipids such as phosphatidylethanolamine, which exhibit negative curvature, making them more prone to deformation and mechanical damage compared to eukaryotic membranes, which are dominated by phosphatidylcholine with zero curvature [96]. In addition, bacterial cell walls contain negatively charged components such as lipopolysaccharides, which enhance the interaction with BP nanosheets [97].

The antibacterial effects of BP can be further enhanced by photothermal activation (BP has a bandgap), which allows for localized antibacterial action under controlled irradiation conditions, although potential thermal damage to surrounding tissues must be considered [98,99]. Based on these different mechanisms, BP shows a broad antibacterial activity against Gram-positive and Gram-negative bacteria, as well as selected fungal pathogens [2,5,39]. Time- and concentration-dependent antibacterial effects have been reported against *E. coli* and *Bacillus subtilis*, while few-layer BP nanoflakes show rapid inhibitory activity against *Pseudomonas aeruginosa*, *Cryptococcus neoformans*, and methicillin-resistant *Staphylococcus aureus* (MRSA) [2,5,39,100]. Notably, laboratory studies suggest that BP-based antibacterial materials can maintain activity during repeated exposure. For example, BPNs retain antibacterial efficacy against *E. coli* over 60 days of sub-lethal exposure, whereas separate studies have reported resistance development to conventional antibiotics, including oxacillin, ofloxacin, and rifampicin, within considerably shorter experimental periods [5,39]. Due to their high drug-loading capacity and surface functionalization potential, other 2D materials like GO and reduced graphene oxide (rGO) are also widely investigated as antibacterial substances [65,101]. However, their biocompatibility is strongly dependent on the particle size, for example nano-sized GO sheets (≈350 nm) induce significantly greater destruction of red blood cells than micrometer-scale sheets and exhibit pronounced cytotoxicity [102]. In contrast, BP seems to offer a distinct balance between antibacterial activity and biological clearance. Rather than acting solely as a passive carrier for drugs, BP directly contributes to the antibacterial efficacy. Its degradation into phosphate ions and mild phosphoric acid (both biologically relevant) represents a natural advantage over other 2D materials [90,103]. This degradation-associated acidification may further inhibit bacterial growth without causing significant cytotoxicity to mammalian cells [90,103]. Importantly, the degradation process may generate reactive oxygen species and other reactive phosphorus intermediates. Therefore, while the decomposition of BP into phosphate species reduces concerns regarding long-term material persistence, this biodegradation process should not be regarded as direct evidence of biosafety.

Similar considerations apply when BP is compared with MXenes and TMDs (see Table 3 for a comparison of antibacterial properties of BP with those of other nanomaterials). MXenes, such as $Ti_3C_2T_x$ (T_x represents surface termination groups such as –OH, –O, and –F), have attracted interest in antibacterial composites due to their high surface area and tuneable surface chemistry [104]; however, their lack of complete biodegradability raises concerns regarding long-term accumulation. TMDs such as MoS_2 and WS_2 offer great chemical stability and photothermal activity [105], but prolonged persistence in biological tissues and uncertain clearance pathways limit their suitability for antimicrobial therapy.

Clinical relevance of black phosphorus in wound healing and infection control

Wound healing is a highly dynamic and multifactorial process that depends on tightly regulated cellular and molecular events to restore damaged tissue. Recent studies indicate that BP nanomaterials can contribute to several stages of wound repair while concurrently suppressing microbial infection [109,110]. Both in vitro and in vivo investigations have reported favourable bio-

Table 3: Antibacterial properties of BP compared to other nanomaterials.

	BP	Graphene/GO	MXenes	TMDs
antibacterial spectrum	broad spectrum: Gram+ and Gram–, fungi [2,5,39]	broad spectrum, good biofilm disruption [106]	broad spectrum [104]	broad spectrum [105]
antibacterial mechanisms	physical damage to bacterial membrane, ROS generation, photothermal effects, acidification upon degradation [2,5,98]	membrane disruption, oxidative stress [106,107]	membrane disruption, oxidative stress, surface-mediated interactions [104]	photothermal effects, ROS generation, membrane interaction [105]
photothermal activity	strong, enhances antibacterial efficacy under mild NIR irradiation [98,99]	moderate, requires high energy for significant PTT [108]	strong hyperthermia effect [104]	strong photothermal response under NIR irradiation [105]
resistance development	low resistance development reported under specific laboratory conditions [5,39]	possible over time [102]	resistance development not well established [104]	resistance development not well established [105]
delivery and formulation strategies	hydrogels, eutectic gels, polymer composites enhance stability and localized delivery [2,5,39]	composite-based formulations to improve stability [101]	incorporated into hydrogels and composites for antibacterial delivery applications [104]	incorporated into nanocomposites and coatings for delivery and photothermal therapy [105]
biodegradability/ clearance	biodegradable into phosphate species [5]	limited biodegradability, long-term clearance remains uncertain [102]	not biodegradable, potential for metal-containing residues [104]	chemically stable, prolonged persistence and unclear clearance pathways [105]

compatibility when BP is administered at optimized concentrations [1,109]. However, supporting data differ between experimental settings. While numerous in vitro studies have evaluated BP across different concentrations and mammalian cell types, in vivo evidence remains comparatively limited and is largely based on preclinical animal models. Although these studies provide encouraging evidence of short-term biocompatibility and wound-healing efficacy, they have not yet investigated long-term safety, biodistribution, clearance, or immune responses. Therefore, promising in vitro biocompatibility cannot necessarily be assumed to translate directly to long-term in vivo safety. Experimental evidence further suggests that BP-based wound dressings can promote cell proliferation and migration, processes that are fundamental to tissue regeneration [111,112]. In addition, degradation products of BP may contribute to the formation of a more favourable local microenvironment by mildly lowering pH, thereby supporting the wound-healing process [109,113]. Besides tissue regeneration BP plays an active role in infection control. Its antimicrobial activity can reduce microbial burden at the wound site, addressing one of the primary causes of delayed healing. A range of BP-based materials have demonstrated substantial activity against bacterial and fungal pathogens by forming protective barriers that limit microbial growth [1,114,115]. This capacity to support tissue repair while preventing infection distinguishes BP-based systems from many conventional wound dressings [39,116].

BP can efficiently convert absorbed light (including daylight and NIR light) into localized heat (vide infra). When carefully controlled, this photothermal effect has been shown to enhance the formation of new blood vessels (angiogenesis) and thus increase blood flow, which facilitates oxygen and nutrient delivery to regenerating tissue [117,118]. These systems achieved temperatures of approximately 50.2 °C, sufficient to support effective bacterial sterilization (93% efficacy). However, excessive thermal exposure, particularly during prolonged NIR irradiation, may induce tissue damage and negatively impact tissue repair. Therefore, current studies have shifted toward the use of mild daylight conditions or short NIR exposures to retain therapeutic benefits while minimizing thermal risk [119].

A broad range of delivery strategies has been explored to apply BP at wound sites, which can be used for different wound types and healing stages. These include microneedle arrays, hydrogel dressings, sprayable formulations, or direct injection [103,111]. Hydrogel dressings are widely applied in acute and chronic wounds, where they act primarily during the inflammatory and proliferative phases by supporting a moist environment, lowering inflammation, and promoting angiogenesis [120]. Injectable hydrogels are particularly suitable for geometrically irregular or infected soft-tissue wounds, enabling localized antibacterial activity during the inflammatory stage while sustaining angiogenic and collagen-remodelling activity in the remodelling phase [113]. Sprayable formulations are advantageous for large surface areas, such as burns or joint-associated wounds, where they form coatings that address early-stage infection while accommodating movement [121]. Microneedle

arrays enable intradermal delivery and are especially relevant for chronic or hypoxic wounds, such as diabetic ulcers, where they can enhance local delivery and support the proliferative stage [122,123].

Mechanisms of antibacterial action

Reactive oxygen species generation and photodynamic therapy

ROS generation is a central antibacterial mechanism of BP, particularly under NIR light irradiation, where generated surface electrons facilitate the production of reactive oxygen species [116,124]. The generated species, including singlet oxygen, hydroxyl radicals, superoxide anions, and hydrogen peroxide can induce oxidative stress within bacterial cells by overcoming their limited antioxidant defences [2,124]. Although mammalian cells possess antioxidant defence systems, BP-induced ROS can also affect these cells, with the extent of cytotoxicity depending on characteristics and concentration of BP, and exposure conditions [116,125-127]. In bacterial cells, ROS-induced oxidative stress leads to the oxidation of bacterial membrane lipids, resulting in membrane damage, increased permeability, and eventual rupture [2,128]. Simultaneously, ROS can cause damage to intracellular proteins and DNA, which disrupts essential metabolic and genetic processes (replication and transcription) ending in bacterial cell death [129,130]. Beyond direct ROS-mediated antibacterial activity, BP nanosheets have also been investigated as photosensitizers in photodynamic therapy (PDT), where light activation is used to deliberately enhance ROS production for bacterial eradication [131]. PDT involves three essential components, namely, BP as the photosensitizer, molecular oxygen, and light irradiation. Together, they facilitate ROS generation that causes oxidative damage to bacterial proteins and nucleic acids, disrupting essential cellular functions and ultimately leading to bacterial cell death [2,131-133]. BPNs are especially suited for PDT due to their tunable direct bandgap, high carrier mobility, and strong NIR absorption, supporting efficient intersystem crossing and singlet oxygen-dominated ROS generation [133]. Unlike conventional photosensitizers (e.g., methylene blue and porphyrin derivatives), BPNs maintain activity in biological environments where other agents often suffer from aggregation and reduced biocompatibility [2,133,134]. The antibacterial efficacy of BP-based PDT systems has been enhanced through composite design. For example, incorporating BPNs into chitosan-based hydrogels helps to achieve over 99% inactivation of *Staphylococcus aureus* and *Escherichia coli* under light exposure, while supporting wound healing in vivo [3,134]. However, PDT's dependence on continuous irradiation remains a limitation, as prolonged exposure may induce phototoxicity, tissue hypoxia, and reduced antibacterial activity once the light is no longer applied (vide supra, wound healing) [131]. To address these challenges, BPNs have been combined with poly(pyridyl methyl styrene) endoperoxide to capture and store ROS generated species during irradiation. These stored reactive species can be released in the dark through thermal decomposition, extending the antimicrobial activity beyond light exposure [2,3,131]. Enhanced PDT effects have also been achieved by combining BPNs with silver nanoparticles (AgNPs). In this system, BP facilitates the reduction of silver ions to AgNPs at defect sites. The produced AgNPs suppress the electron–hole recombination during the PDT process, resulting in enhanced ROS production and sustained antibacterial action [1,2,135]. Notably, compared to carbon-based materials like GO, BP-based systems show superior performance in PDT since GO lacks a tunable bandgap and exhibits limited light absorption, restricting ROS generation [136,137]. Furthermore, GO has additional limitations, including size-dependent variability in antibacterial activity, aggregation under certain ionic conditions, and potential biocompatibility concerns that depend on its physicochemical properties and exposure route [54,138-141].

A recent study suggests that low concentrations of BP nanosheets can enhance the horizontal transfer of antibiotic resistance genes (ARGs), a process by which resistance genes are exchanged between bacteria during bacterial conjugation, particularly at low, non-lethal concentrations (0.0001–1 mg/L) [142]. This effect is linked to increased ROS production, lipid peroxidation, and activation of the SOS DNA damage response (a bacterial repair mechanism triggered by DNA damage that promotes plasmid uptake). However, at higher BP nanosheet concentrations, excessive oxidative stress suppresses conjugative transfer. These findings highlight the dual role of black phosphorus nanosheets (BPNSs), where bactericidal effects occur at higher doses, while sub-lethal doses may inadvertently encourage ARG spread [142].

Photothermal therapy

Due to its layer-dependent and adjustable bandgap (0.3–2.0 eV), BP exhibits a broad optical absorption spanning the visible-to-NIR region, enabling efficient conversion of light into localized heat [2,113]. This photothermal effect allows local hyperthermia treatments to disrupt bacterial membranes while minimizing damage to surrounding healthy tissue [7,143]. Stronger NIR irradiation further enhances the clinical relevance of BP-based photothermal therapy (PTT) by allowing deeper tissue penetration and reduced scattering (compared with ultraviolet or visible light), enabling non-invasive treatment of subdermal infections [2,7,116].

BP is more suitable for NIR-based antibacterial therapy than ZnO, Ag, and Cu nanoparticles, which mainly rely on visible

light and respond poorly to NIR. ZnO shows very limited NIR absorption with a band gap of ≈3.37 eV [2,144]. In contrast, BP's layered structure allows for precise tuning of optical properties to match NIR wavelengths within the therapeutic window (700–1100 nm), resulting in high photothermal conversion efficiency [2,143,145]. The photothermal activity of BP can be further amplified through doping of the BP structure with other nanoparticles. For example, BP/gold nanocomposites (BPN/AuNPs) exhibit enhanced antibacterial activity under NIR irradiation relative to pristine BP [146]. Similarly, BP/carbon quantum dot nanocomposites (BP@CQDs) exhibit enhanced treatment efficiency by achieving simultaneous PDT and PTT antibacterial effects [144].

To optimize the localized delivery and therapeutic retention of BP, it has also been incorporated into biomaterial carriers like hydrogels, which help minimize unnecessary exposure and promote accumulation at infection sites [113,116,147]. For example, a galactose/BP/kanamycin composite (Gal-BPN@Kana) combines targeted bacterial recognition with BP-mediated PTT under NIR irradiation, achieving complete wound closure within nine days in a *Pseudomonas aeruginosa*-infected wound model. In this system, photothermal heating also facilitates the controlled release of kanamycin, resulting in synergistic antibacterial activity. This composite combines three antibacterial mechanisms, that is, ROS generation, PTT, and controlled drug release (Figure 2) [2,126,148].

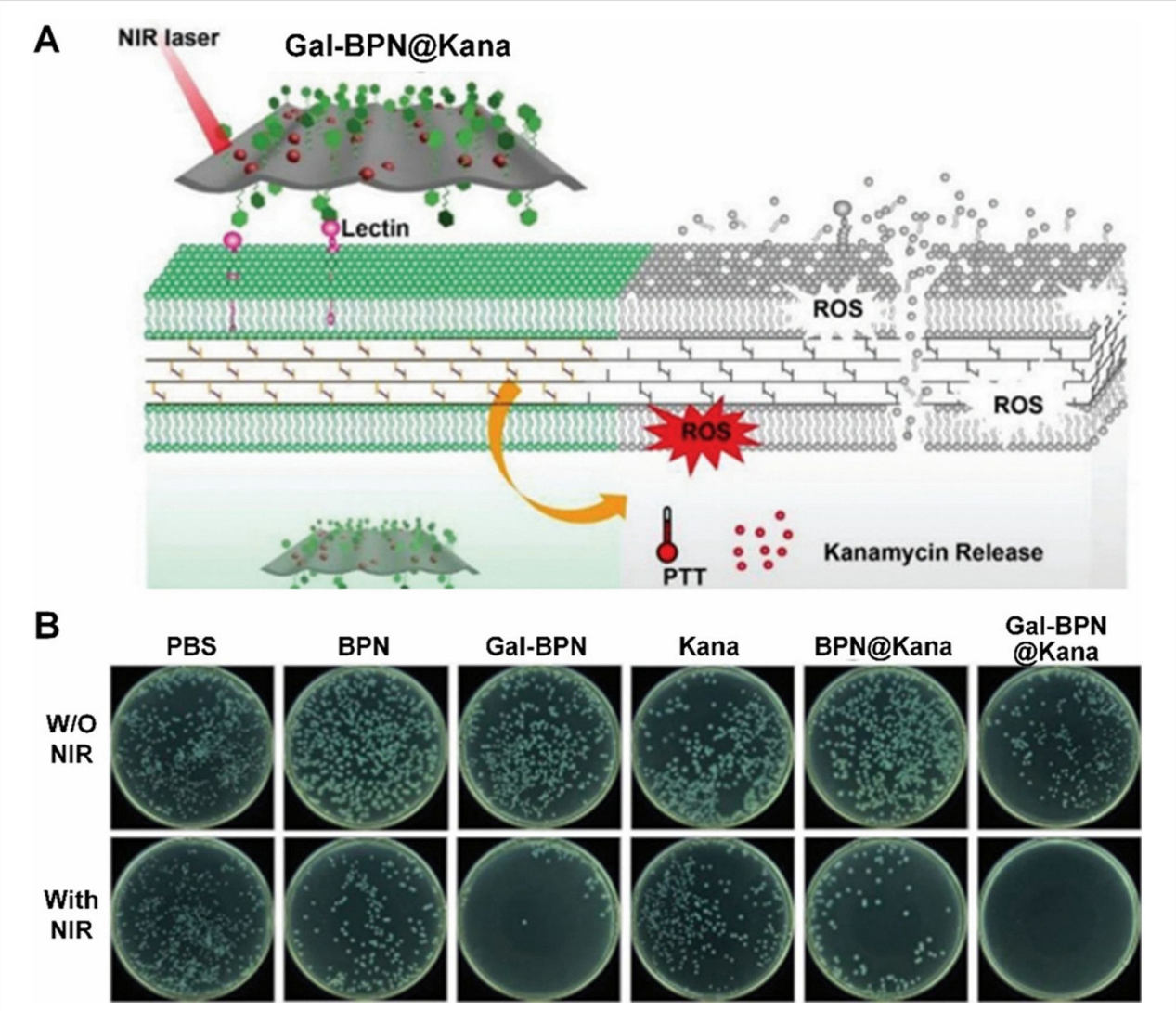

Figure 2: (A) Antibacterial mechanism of galactose-functionalized black phosphorus nanosheets loaded with kanamycin (Gal-BPN@Kana). (B) *P. aeruginosa* colony growth on agar plates following treatment with phosphate-buffered saline (PBS), black phosphorus nanosheets (BPN), galactose-functionalized BPN (Gal-BPN), kanamycin (Kana), BPN loaded with kanamycin (BPN@Kana), and Gal-BPN@Kana, each tested with and without near-infrared (NIR) irradiation. Figure 2 was reproduced from [148], Z. Guo et al., "Multifunctional Glyco-Nanosheets to Eradicate Drug-Resistant Bacteria on Wounds", *Adv. Healthcare Mater.*, with permission from John Wiley and Sons. Copyright © 2020 WILEY-VCH Verlag GmbH & Co. KGaA, Weinheim. This content is not subject to CC BY 4.0.

The nanoknife effect

BP nanosheets exhibit potent antibacterial activity through a contact-dependent physical mechanism known as the nanoknife effect (Figure 3). This effect operates independently of ROS generation or photothermal activation [2]. Like other 2D materials such as graphene and GO, BP can mechanically disrupt bacterial membranes upon direct contact. The unique structural and physicochemical features of BP nanoflakes (sharp edges) often lead to extremely high antibacterial efficiency [2,149].

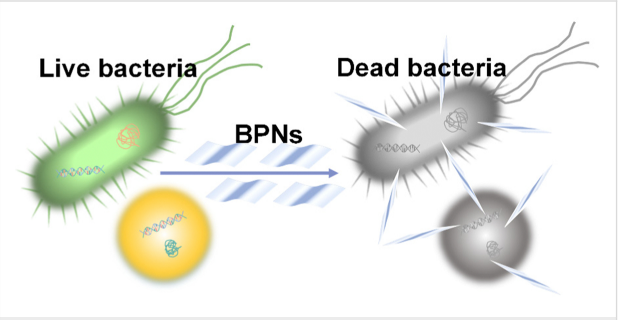

Figure 3: Schematic illustration of the antibacterial nanoknife mechanism of black phosphorus nanosheets against bacterial cells. Reproduced with permission from [2], © The Royal Society of Chemistry 2023. This content is not subject to CC BY 4.0.

The puckered crystal lattice and high mechanical stiffness of BP nanosheets concentrate forces at the sharp edges, enabling effective penetration and slicing of bacterial lipid bilayers [150]. This localized mechanical stress at the nanosheet/membrane interface leads to membrane rupture, cytoplasmic leakage, and finally bacterial cell death [2,149]. Experimental studies support this purely physical mechanism [150]. For example, Guo et al. confirmed severe membrane damage and RNA leakage by transmission electron microscopy when *E. coli* (Gram-negative) and *S. aureus* (Gram-positive) were treated with BPNs [149]. Consistently, Liu et al. observed that more than 90% of *E. coli* cells were killed within two hours of dark exposure to BPNSs. This activity was stopped when BPNSs were confined within dialysis membranes, confirming that direct contact is essential for nanoknife-mediated killing [151]. Quantitative studies further demonstrate concentration-dependent antibacterial effects. BP concentrations between 25 and 100 μg/mL produce progressively stronger inhibition of *E. coli* growth, with complete suppression at higher concentrations [88,152,153]. Compared with carbon-based 2D materials, BP offers distinct advantages for contact-mediated antibacterial action. BP achieves comparable or superior efficacy at lower concentrations than GO or rGO, which typically require more than 100 μg/mL for similar effects [5,152]. Potentially, BP's natural surface hydrophilicity enables stronger interactions with bacterial membranes than other materials like graphene, resulting in enhanced mechanical antibacterial efficiency [2,4]. Notably, the nanoknife effect of BP is especially relevant for biomedical applications where light-based activation is impractical, including wound dressings, implant coatings, and surgical sutures [154].

BP composite materials for enhanced antibacterial action

Metal-containing BP composites often show enhanced antibacterial efficacy through synergistic mechanisms combining photothermal effects, ROS generation, and improved bacterial interaction under NIR irradiation [6,155]. Analogously, polymer-functionalized BP composites improve colloidal stability, targeted delivery to infection sites and enable sensitivity to external stimuli, thereby amplifying antibacterial performance and tissue repair [93]. To provide a concise overview of these BP composites, important examples of metal- and polymer-modified BP materials are summarized in Table 4 and Table 5, respectively. The listed examples highlight how the modification of BP with metals or polymers can improve targeted delivery, mechanism of action and thus antibacterial efficacy. Beyond single-metal modifications, multimetallic BP-based nanocomposites have been shown to even further enhance antibacterial efficacy. For example, BP/ZnO/Ag composites exhibit exceptionally low minimum inhibitory concentration values (≈12.5 μg/mL) against drug-resistant *Acinetobacter baumannii*, reflecting cooperative contributions from metal ion release, ROS generation, and membrane disruption [93].

As an example of polymer-integrated BP composite materials, AI-MPDA@BP (composed of BP nanosheets, mesoporous polydopamine (MPDA), L-arginine (L-Arg), and indocyanine green (ICG)) enables antibacterial therapy through combined PTT, PDT, and nitric oxide release [160]. This multimodal mechanism results in up to 95% bactericidal efficacy against *Staphylococcus aureus* and enables complete wound closure within 14 days, highlighting the potential of polymer-functionalized BP systems for antibiotic-free infection control [160]. Overall, metal- and polymer-modified BP composites enhance antibacterial efficacy by coupling PTT/PDT effects with ROS generation and show improved material stability. Together, these enable controlled metal ion (e.g., Ag^+, Zn^{2+}) and NO-mediated interactions, leading to efficient bacterial extinction and reduced antibiotic dependence. This is critical in the fight against antimicrobial resistance. Ag^+ and Zn^{2+} contribute to membrane-disruptive antibacterial effects, while NO exerts bactericidal activity via direct DNA damage and through reaction with photodynamically generated ROS. The latter reaction delivers peroxynitrite ($ONOO^-$), a potent oxidant capable of further membrane disruption. Importantly both, metal ion release and NO generation are stimulus-responsive (activated by NIR or ROS) and therefore off-target effects may be mini-

Table 4: BP/metal composites with antibacterial activity.

BP/metal composite	Strategy	Mechanism	Application	Study outcome
BP/Au [5]	AuNPs are synthesized in situ from a gold salt on the BP surface (reduction potential of BP is sufficient)	enhanced PTT activity, ROS amplification, improved stability of the composite	antibacterial coatings, sensing probes	photothermal conversion increased by Au doping from 12.9 to 43.6%, 100% bacterial kill rate
BP/Bi_2O_3 [5]	Bi_2O_3 fills defect sites in BP to form heterojunction, surface coated with polylysine	combines PTT and PDT antibacterial effects	chronic wound treatment, especially diabetic infections	100% inhibition of *P. aeruginosa*, *S. aureus*, and *E. coli* under NIR irradiation
BP/Ti-SA4 [5]	titanium aminobenzenesulfonic acid (Ti-SA4) anchored on BP surface via strong P–Ti bonding	kills bacteria directly, even without light activation	non-light-triggered antibacterial treatment	eliminates most bacteria within 3 h, more potent than Ti-SA4 alone
BP/Cu [5,156]	Cu is loaded onto BP via reduction of a copper salt with $NaBH_4$	ROS production boosts antibacterial effects	broad-spectrum of antibacterial applications	enhanced ROS generation and severe bacterial membrane damage
BP/Mg in GelMA hydrogel [5]	Mg-doped BP added to a GelMA hydrogel matrix for enhanced photoconductivity	ROS burst, anti-inflammatory, promotes Schwann cell migration and tissue repair	neural tissue healing and antibacterial bone implants	reduces inflammation and encourages nerve regeneration
BP/ZnO on titanium [5]	BP/ZnO hybrid coating on titanium implant surface	NIR-triggered ROS generation and Zn^{2+} release, PTT-enhanced immune modulation	implant antibacterial surface coating	ROS increased by 41.5% (*S. aureus*) and 36.3% (*E. coli*) under NIR compared with single-agent or non-irradiated controls, antibacterial rate reached 98% (*S. aureus*) and 97% (*E. coli*) under NIR irradiation
BP/PDA/ZnO on NiTi alloy [157]	BP and ZnO NPs deposited onto NiTi alloy with polydopamine (PDA) coating	PTT bacteriostasis under 808 nm NIR combined with PTT-enhanced Zn^{2+} release	antibacterial surface modification for NiTi bone implants to prevent postoperative infection	antibacterial rate up to 93.8% in vitro
BP/Sr [7]	Sr^{2+} ions electrostatically assembled onto BP nanosheets to enhance bacterial interaction	PTT bacterial killing under NIR, Sr^{2+} improves bacterial adhesion and membrane disruption	infected wound treatment, soft tissue regeneration	≥99% bacterial extinction against *S. aureus* and *E. coli* under 808 nm NIR, accelerated wound healing
BP/Prussian blue/Ti [158]	BP/Prussian blue nanohybrids immobilized on Ti with a polydopamine adhesive layer	NIR-triggered photothermal killing combined with nanozyme-mediated ROS scavenging, Prussian blue mimics antioxidant enzymes	antibacterial titanium implant coatings	99.8% (*E. coli*) and 99.3% (*S. aureus*) inhibition under 808 nm NIR, photothermal temperature up to 59.6 °C
BP/CeO_2/Pluronic F127 hydrogel [159]	CeO_2 nanoparticles integrated with BP nanosheet embedded in thermoresponsive PF127 hydrogel	BP-mediated photothermal killing under NIR combined with Ce^{3+}/Ce^{4+} redox-driven ROS scavenging	post-surgical and infected wound treatment	93% reduction in bacteria, no systemic toxicity

mized. Although Table 4 and Table 5 demonstrate promising antibacterial activity of different BP composite materials, direct comparison between studies remains challenging because of differences in BP formulation, bacterial morphology, concentration, bacterial models, irradiation conditions, and antibacterial assessment methods. Consequently, differences in reported antibacterial efficacy cannot necessarily be attributed to the superiority of one BP formulation over another.

Table 5: BP/polymer composites with antibacterial activity.

Polymer(s)	Design and mechanism	Targeted bacteria	Study outcome
gelatin methacryloyl (GelMA) [5]	BP nanosheets embedded in UV-crosslinked GelMA via electrostatic interaction	*S. aureus*	up to 98% bacterial extinction, improved hydrogel strength and antibacterial response
polyvinyl alcohol (PVA), sodium alginate (ALG) [5]	BP-based hydrogel with PDT and PTT activity	MRSA	≈90% inhibition, upregulated vascular endothelial growth factor (VEGF) and basic fibroblast growth factor (bFGF) expression for tissue repair
PLGA scaffold [5]	BP encapsulated in biodegradable matrix. NIR-triggered release	not specified	99% bacterial clearance after three weeks, improved photothermal action
polydopamine (PDA) [5]	BP/PDA coating on Ti, enhanced NIR absorbance	*S. aureus*	96.6% eradication under enhanced photothermal conditions
chitosan, polycaprolactone (PCL), PDA [5]	chloroplast-inspired hybrid scaffold with stable NIR-triggered photothermal performance	not specified	high, NIR-triggered antibacterial activity and high thermal stability
quaternary ammonium salt chitosan (QCS), hyaluronic acid, poly L-lactic acid (PLLA) nanofibres [5]	QCS enhanced BP- PTT sensitivity and improved oxygen transport to alleviate hypoxia	MRSA, *E. coli*	>98% MRSA and 90% *E. coli* eradication
EGCG (tea polyphenols) [5]	EGCG conjugated to BPQDs to boost ROS generation and promote angiogenesis	not specified	improved PDT via VEGF/bFGF expression, ROS enhanced
ε-polylysine [5]	tight adhesion to bacterial membranes, membrane disruption, and BP hyperthermia	not specified	strong membrane-targeted killing with improved BP biocompatibility and stability
polysaccharides from *Elaeagnus mollis* [5]	BP/polysaccharide composite improved stability and inhibited virulence factor expression and biofilm formation	*S. aureus*	99.999% eradication in 60 min under light
mesoporous polydopamine (MPDA), L-arginine (L-Arg), indocyanine green (ICG) [160]	BPNSs integrated with MPDA, L-Arg, and ICG; combined PTT, PDT, and nitric oxide release	*S. aureus*	≈95% bactericidal efficacy, complete wound healing within 14 days

Finally, to conclude this section on the different mechanisms of action, we refer the reader to Table 6, which categorizes the various antimicrobial effects into those that can be achieved by pristine BP and those that can only be realised through BP-based composite materials.

Conclusion

The accelerating global burden of antimicrobial resistance highlights the urgent need for antibacterial strategies that extend beyond conventional antibiotics and single-mechanism agents. Black phosphorus addresses several fundamental limitations as-

Table 6: Intrinsic antibacterial effects of pristine BP versus effects arising from BP composites.

Antibacterial effects of pristine BP	Antibacterial effects enabled by BP composites
ROS generation, particularly under light irradiation (PDT)	metal-ion release (e.g., Ag^+ and Zn^{2+}) from incorporated metal-containing components
nanoknife effect: physical disruption of bacterial membranes by sharp BP nanosheet edges	nitric oxide (NO) generation from incorporated NO-releasing components
photothermal effect under NIR irradiation, causing localized thermal damage (PTT)	controlled antibiotic release (e.g., kanamycin) from BP-based drug-delivery composites
–	enhanced ROS generation and/or photothermal activity through composite modification (e.g., AgNPs, AuNPs, CQDs)

sociated with existing antimicrobial nanomaterials. A key advantage of BP lies in its biodegradability, whereby it decomposes into biologically benign phosphate species. This distinguishes BP from bio-persistent materials such as GO and many metal-based nanomaterials, which raise concerns regarding long-term accumulation, cytotoxicity, and environmental impact. Although BP's sensitivity to oxygen and moisture presents a practical challenge, advances in surface passivation, polymer encapsulation, and heterostructure formation have proven effective in stabilizing BP for therapeutic timescales without compromising its degradability.

Importantly, BP's antibacterial performance arises from multimodal and targeted reactivity, rather than reliance on a bactericidal pathway. Unlike conventional antibiotics that act on discrete molecular targets, BP employs simultaneous physical and chemical stress on bacterial cells. BP nanosheets trigger potent, contact-dependent physical disruption of bacterial membranes via the nanoknife effect, enabling effective antibacterial action even in the absence of external stimuli. Under light activation, BP initiates ROS generation, leading to oxidative damage of bacterial membranes, proteins, and genetic material. In parallel, BP's strong absorption in the near-infrared region enables efficient photothermal heating, supporting localized hyperthermia treatment and non-aggressive bacterial eradication. These complementary mechanisms may reduce reliance on a single antibacterial target; however, whether they reduce the risk of long-term resistance development remains to be established.

Combination with silver, gold, copper, or zinc oxide, as well as incorporation into polymeric matrices including hydrogels, chitosan, and polydopamine-based systems, substantially enhances the antibacterial performance of BP. Such hybrid materials exhibit stability, allow for localized delivery and support tissue repair in infected environments. Together, surface passivation, chemical modification, elemental doping, and formulation strategies with polymers can enhance the stability of BP while preserving its reactivity, enabling practical application in antimicrobial therapies and regenerative medicine. Continued refinement of stabilization approaches and deeper understanding of degradation pathways remain essential for unlocking the full clinical potential of black phosphorus. Despite these advances, several challenges remain before BP-based antibacterial systems can progress towards clinical translation. Scalable and reproducible production of materials with consistent physicochemical characteristics is important since different synthesis approaches can affect material quality and structure. Greater standardization of material characterization and antibacterial evaluation is needed to enable meaningful comparison between BP formulations and studies. Furthermore, stabilization strategies should balance sufficient therapeutic stability with controlled degradation under biologically relevant conditions, rather than simply maximizing BP stability. Currently, long-term in vivo safety is poorly understood, particularly with respect to dose- and formulation-dependent toxicity, biodistribution, and clearance. Although laboratory studies suggest that BP may retain antibacterial activity upon repeated exposure, evidence for long-term resistance development remains limited and emerging findings on antibiotic-resistance-gene transfer under sub-lethal BP exposure warrant further investigation. Ultimately, successful clinical translation of BP will require overcoming manufacturing, characterization, efficacy, and safety challenges while meeting the relevant regulatory requirement.

Funding

D.H. acknowledges support of the Marie Skłodowska-Curie Actions Staff Exchanges (UKRI project number 101131382), CLEANWATER funded by the European Union under the Horizon-Europe Programme.

Author Contributions

Paniz Olapour: visualization; writing – original draft; writing – review & editing. Dominikus Heift: conceptualization; supervision; visualization; writing – review & editing.

ORCID® iDs

Paniz Olapour - https://orcid.org/0009-0002-6578-7388
Dominikus Heift - https://orcid.org/0000-0002-6799-5052

Data Availability Statement

Data sharing is not applicable as no new data was generated or analyzed in this study.

References

1. Ouyang, J.; Liu, R.-Y.; Chen, W.; Liu, Z.; Xu, Q.; Zeng, K.; Deng, L.; Shen, L.; Liu, Y.-N. *J. Mater. Chem. B* **2018,** *6,* 6302–6310. doi:10.1039/c8tb01669k
2. Xu, Y.; Chen, S.; Zhang, Y.; Wu, C.; Li, L.; Hu, X.; Zhang, J.; Wang, Y. *J. Mater. Chem. B* **2023,** *11,* 7069–7093. doi:10.1039/d3tb00723e
3. Zhang, Y.; Qu, X.-F.; Zhu, C.-L.; Yang, H.-J.; Lu, C.-H.; Wang, W.-L.; Pang, Y.; Yang, C.; Chen, L.-J.; Li, X.-F. *ACS Appl. Bio Mater.* **2021,** *4,* 4821–4832. doi:10.1021/acsabm.1c00054
4. Gerile, S.; Shen, Q.; Kang, J.; Liu, W.; Dong, A. *Colloids Surf., B* **2024,** *241,* 114037. doi:10.1016/j.colsurfb.2024.114037
5. Zhang, L.; You, J.; Lv, H.; Liu, M.; Quni, S.; Liu, X.; Zhou, Y. *Int. J. Nanomed.* **2023,** *18,* 6563–6584. doi:10.2147/ijn.s438448
6. Naskar, A.; Cho, H.; Kim, K.-s. *J. Compos. Sci.* **2023,** *7,* 423. doi:10.3390/jcs7100423

7. Yu, G.; Zhang, S.; Chen, J.; Lian, G.; Zhong, J.; Liu, Y.; Xu, X. *J. Biomater. Appl.* **2026,** *40,* 916–925. doi:10.1177/08853282251376879
8. Kumar, P.; Huo, P.; Zhang, R.; Liu, B. *Nanomaterials* **2019,** *9,* 737. doi:10.3390/nano9050737
9. Rasool, K.; Helal, M.; Ali, A.; Ren, C. E.; Gogotsi, Y.; Mahmoud, K. A. *ACS Nano* **2016,** *10,* 3674–3684. doi:10.1021/acsnano.6b00181
10. Zhao, Y.; Jia, Y.; Xu, J.; Han, L.; He, F.; Jiang, X. *Chem. Commun.* **2021,** *57,* 2998–3001. doi:10.1039/d1cc00327e
11. Liu, X.; Zhao, X.; Qiu, H.; Liang, W.; Liu, L.; Sun, Y.; Zhao, L.; Wang, X.; Liang, H. *Materials* **2025,** *18,* 1889. doi:10.3390/ma18081889
12. Gnanasekar, S.; He, X.; Nagay, B. E.; Xu, K.; Rao, X.; Duan, S.; Murugesan, S.; Barão, V. A. R.; Kang, E.-T.; Xu, L. *Bioact. Mater.* **2025,** *51,* 150–176. doi:10.1016/j.bioactmat.2025.05.002
13. Chen, H.; Wang, Y.; Chen, X.; Wang, Z.; Wu, Y.; Dai, Q.; Zhao, W.; Wei, T.; Yang, Q.; Huang, B.; Li, Y. *Molecules* **2024,** *29,* 2902. doi:10.3390/molecules29122902
14. Li, P.; Zhai, Y.; Liu, J.; Dai, Y.; Li, D.; Zhang, S. *Sci. Rep.* **2025,** *15,* 9266. doi:10.1038/s41598-025-93489-1
15. Wang, G.; Wang, T.; Dang, Y.; Lu, Z.; Su, G.; Feng, B.; Zhuo, Y.; Jiang, X.; Ye, Q.; Wu, C.; Pu, X.; Zhao, Y.; Zhao, X.; Cai, S.; Du, S.; Jia, S.; Wang, Y.; Wu, D.; Rao, H.; Sun, M. *Chem. Eng. J.* **2023,** *461,* 141959. doi:10.1016/j.cej.2023.141959
16. Konopatsky, A. S.; Kotyakova, K. Y.; Varlamova, L. A.; Barilyuk, D. V.; Teplyakova, T. O.; Antipina, L. Y.; Sorokin, P. B.; Wang, C.; Shtansky, D. V. *Ceram. Int.* **2024,** *50,* 33846–33855. doi:10.1016/j.ceramint.2024.06.203
17. Antipina, L. Y.; Kotyakova, K. Y.; Tregubenko, M. V.; Shtansky, D. V. *Nanomaterials* **2022,** *12,* 3157. doi:10.3390/nano12183157
18. Casals, E.; Gusta, M. F.; Bastus, N.; Rello, J.; Puntes, V. *Microorganisms* **2025,** *13,* 952. doi:10.3390/microorganisms13040952
19. Negi, P.; Chadha, J.; Harjai, K.; Gondil, V. S.; Kumari, S.; Raj, K. *Biomedicines* **2024,** *12,* 1104. doi:10.3390/biomedicines12051104
20. Rizvi, S. M. D.; Lila, A. S. A.; Moin, A.; Hussain, T.; Kamal, M. A.; Sonbol, H.; Khafagy, E.-S. *Pharmaceutics* **2023,** *15,* 430. doi:10.3390/pharmaceutics15020430
21. Dykman, L.; Khlebtsov, B.; Khlebtsov, N. *Adv. Drug Delivery Rev.* **2025,** *216,* 115481. doi:10.1016/j.addr.2024.115481
22. Ma, X.; Zhou, S.; Xu, X.; Du, Q. *Front. Surg.* **2022,** *9,* 905892. doi:10.3389/fsurg.2022.905892
23. Youn, S.-M.; Choi, S.-J. *Int. J. Mol. Sci.* **2022,** *23,* 6074. doi:10.3390/ijms23116074
24. Mendes, C. R.; Dilarri, G.; Forsan, C. F.; Sapata, V. d. M. R.; Lopes, P. R. M.; de Moraes, P. B.; Montagnolli, R. N.; Ferreira, H.; Bidoia, E. D. *Sci. Rep.* **2022,** *12,* 2658. doi:10.1038/s41598-022-06657-y
25. Vasiliev, G.; Kubo, A.-L.; Vija, H.; Kahru, A.; Bondar, D.; Karpichev, Y.; Bondarenko, O. *Sci. Rep.* **2023,** *13,* 9202. doi:10.1038/s41598-023-36460-2
26. Mei, L.; Zhu, S.; Yin, W.; Chen, C.; Nie, G.; Gu, Z.; Zhao, Y. *Theranostics* **2020,** *10,* 757–781. doi:10.7150/thno.39701
27. Liu, H.; Xing, F.; Zhou, Y.; Yu, P.; Xu, J.; Luo, R.; Xiang, Z.; Maria Rommens, P.; Liu, M.; Ritz, U. *Mater. Des.* **2023,** *233,* 112231. doi:10.1016/j.matdes.2023.112231
28. Yu, X.; Xu, C.; Sun, J.; Xu, H.; Huang, H.; Gan, Z.; George, A.; Ouyang, S.; Liu, F. *J. Nanobiotechnol.* **2024,** *22,* 515. doi:10.1186/s12951-024-02785-x
29. Zhao, J.; Wu, H.; Zhao, J.; Yin, Y.; Zhang, Z.; Wang, S.; Lin, K. *J. Nanobiotechnol.* **2021,** *19,* 36. doi:10.1186/s12951-020-00763-7
30. Kang, K.; Wang, L.; Yu, K.; Ma, Y.; Qu, F.; Lin, H. *Biomater. Adv.* **2023,** *144,* 213168. doi:10.1016/j.bioadv.2022.213168
31. Liu, H.; Du, Y.; Deng, Y.; Ye, P. D. *Chem. Soc. Rev.* **2015,** *44,* 2732–2743. doi:10.1039/c4cs00257a
32. Tian, H.; Wang, J.; Lai, G.; Dou, Y.; Gao, J.; Duan, Z.; Feng, X.; Wu, Q.; He, X.; Yao, L.; Zeng, L.; Liu, Y.; Yang, X.; Zhao, J.; Zhuang, S.; Shi, J.; Qu, G.; Yu, X.-F.; Chu, P. K.; Jiang, G. *Chem. Soc. Rev.* **2023,** *52,* 5388–5484. doi:10.1039/d2cs01018f
33. Boidi, G.; Ronai, B.; Heift, D.; Benini, F.; Varga, M.; Righi, M. C.; Rosenkranz, A. *Adv. Colloid Interface Sci.* **2024,** *328,* 103180. doi:10.1016/j.cis.2024.103180
34. Galicia Hernandez, J. M.; Fernandez-Escamilla, H. N.; Guerrero Sanchez, J.; Takeuchi, N. *Sci. Rep.* **2022,** *12,* 20979. doi:10.1038/s41598-022-24425-w
35. Golias, E.; Krivenkov, M.; Varykhalov, A.; Sánchez-Barriga, J.; Rader, O. *Nano Lett.* **2018,** *18,* 6672–6678. doi:10.1021/acs.nanolett.8b01305
36. Zhang, W.; Enriquez, H.; Tong, Y.; Mayne, A. J.; Bendounan, A.; Smogunov, A.; Dappe, Y. J.; Kara, A.; Dujardin, G.; Oughaddou, H. *Nat. Commun.* **2021,** *12,* 5160. doi:10.1038/s41467-021-25262-7
37. Rybkovskiy, D. V.; Lepeshkin, S. V.; Baturin, V. S.; Mikhailova, A. A.; Oganov, A. R. *Nanoscale* **2023,** *15,* 1338–1346. doi:10.1039/d2nr06523a
38. Passaglia, E.; Sgarbossa, A. *Pharmaceutics* **2023,** *15,* 2748. doi:10.3390/pharmaceutics15122748
39. Smith, L. S.; Haidari, H.; Amsalu, A.; Howarth, G. S.; Bryant, S. J.; Walia, S.; Elbourne, A.; Kopecki, Z. *Int. J. Mol. Sci.* **2024,** *25,* 12824. doi:10.3390/ijms252312824
40. Qiao, J.; Kong, X.; Hu, Z.-X.; Yang, F.; Ji, W. *Nat. Commun.* **2014,** *5,* 4475. doi:10.1038/ncomms5475
41. Lu, W.; Ma, X.; Fei, Z.; Zhou, J.; Zhang, Z.; Jin, C.; Zhang, Z. *Appl. Phys. Lett.* **2015,** *107,* 021906. doi:10.1063/1.4926731
42. Du, H.; Lin, X.; Xu, Z.; Chu, D. *J. Mater. Chem. C* **2015,** *3,* 8760–8775. doi:10.1039/c5tc01484k
43. Sun, Z.; Zhang, Y.; Yu, H.; Yan, C.; Liu, Y.; Hong, S.; Tao, H.; Robertson, A. W.; Wang, Z.; Pádua, A. A. H. *Nanoscale* **2018,** *10,* 12543–12553. doi:10.1039/c8nr03513j
44. Liu, H.; Mei, Y.; Zhao, Q.; Zhang, A.; Tang, L.; Gao, H.; Wang, W. *Pharmaceutics* **2021,** *13,* 1344. doi:10.3390/pharmaceutics13091344
45. Devi P, K.; Jose K, M.; Singh, K. K.; Gaidhane, V. H.; Sood, N.; Bhalla, N. *Nanoscale Horiz.* **2026,** *11,* 662–700. doi:10.1039/d5nh00429b
46. Tatullo, M.; Genovese, F.; Aiello, E.; Amantea, M.; Makeeva, I.; Zavan, B.; Rengo, S.; Fortunato, L. *Materials* **2019,** *12,* 2301. doi:10.3390/ma12142301
47. Nilges, T.; Kersting, M.; Pfeifer, T. *J. Solid State Chem.* **2008,** *181,* 1707–1711. doi:10.1016/j.jssc.2008.03.008
48. Sun, J.; Zheng, G.; Lee, H.-W.; Liu, N.; Wang, H.; Yao, H.; Yang, W.; Cui, Y. *Nano Lett.* **2014,** *14,* 4573–4580. doi:10.1021/nl501617j
49. Pedersen, S. V.; Muramutsa, F.; Wood, J. D.; Husko, C.; Estrada, D.; Jaques, B. J. *npj 2D Mater. Appl.* **2020,** *4,* 36. doi:10.1038/s41699-020-00170-4
50. Bawadkji, O. Black Phosphorus Nanomaterials for Biomedical Applications and Precious Metal Recovery. Ph.D. Thesis, Freie Universität Berlin, Berlin, Germany, 2024.
51. Ozawa, A.; Yamamoto, M.; Tanabe, T.; Hosokawa, S.; Yoshida, T. *J. Mater. Chem. A* **2020,** *8,* 7368–7376. doi:10.1039/c9ta13441g
52. Qian, X.; Gu, Z.; Chen, Y. *Mater. Horiz.* **2017,** *4,* 800–816. doi:10.1039/c7mh00305f

53. Wang, S.; Yang, X.; Zhou, L.; Li, J.; Chen, H. *J. Mater. Chem. B* **2020,** *8,* 2974–2989. doi:10.1039/c9tb02845e
54. Ghulam, A. N.; dos Santos, O. A. L.; Hazeem, L.; Pizzorno Backx, B.; Bououdina, M.; Bellucci, S. *J. Funct. Biomater.* **2022,** *13,* 77. doi:10.3390/jfb13020077
55. Fan, T.; Yan, L.; He, S.; Hong, Q.; Ai, F.; He, S.; Ji, T.; Hu, X.; Ha, E.; Zhang, B.; Li, Z.; Zhang, H.; Chen, X.; Hu, J. *Chem. Soc. Rev.* **2022,** *51,* 7732–7751. doi:10.1039/d1cs01070k
56. Chen, L.; Dai, X.; Feng, W.; Chen, Y. *Acc. Mater. Res.* **2022,** *3,* 785–798. doi:10.1021/accountsmr.2c00025
57. Xiong, S.-W.; Fu, P.-g.; Zou, Q.; Chen, L.-y.; Jiang, M.-y.; Zhang, P.; Wang, Z.-g.; Cui, L.-s.; Guo, H.; Gai, J.-G. *ACS Appl. Mater. Interfaces* **2021,** *13,* 196–206. doi:10.1021/acsami.0c17800
58. Sengul, A. B.; Asmatulu, E. *Environ. Chem. Lett.* **2020,** *18,* 1659–1683. doi:10.1007/s10311-020-01033-6
59. Yoon, J.; Kim, S.; Park, K. H.; Lee, S.; Kim, S. J.; Lee, H.; Oh, T.; Koo, C. M. *Small Methods* **2023,** *7,* 202201579. doi:10.1002/smtd.202201579
60. Sirelkhatim, A.; Mahmud, S.; Seeni, A.; Kaus, N. H. M.; Ann, L. C.; Bakhori, S. K. M.; Hasan, H.; Mohamad, D. *Nano-Micro Lett.* **2015,** *7,* 219–242. doi:10.1007/s40820-015-0040-x
61. Liu, Z.; Zhao, J.; Yin, L.; Wang, K.; Feng, H.; Li, L.; Xiong, S.; Li, X.; Liu, X.; Dai, Y.; Yue, T.; Wang, Z.; Xing, B. *Environ. Sci. Technol.* **2025,** *59,* 4832–4844. doi:10.1021/acs.est.4c13298
62. Wu, P.; Cui, P.; Du, H.; Alves, M. E.; Liu, C.; Zhou, D.; Wang, Y. *ACS Earth Space Chem.* **2019,** *3,* 495–502. doi:10.1021/acsearthspacechem.8b00165
63. Shi, M.; de Mesy Bentley, K. L.; Palui, G.; Mattoussi, H.; Elder, A.; Yang, H. *Nanoscale* **2017,** *9,* 4739–4750. doi:10.1039/c6nr09102d
64. Mbanga, O.; Cukrowska, E.; Gulumian, M. *Toxicol. Rep.* **2022,** *9,* 788–796. doi:10.1016/j.toxrep.2022.03.044
65. Bellier, N.; Baipaywad, P.; Ryu, N.; Lee, J. Y.; Park, H. *Biomater. Res.* **2022,** *26,* 65. doi:10.1186/s40824-022-00313-2
66. Anju, S.; Ashtami, J.; Mohanan, P. V. *Mater. Sci. Eng., C* **2019,** *97,* 978–993. doi:10.1016/j.msec.2018.12.146
67. Xie, H.; Chen, Z.; Zhang, N.; Wu, F.; Su, H.; Liu, Y.; Xie, D.; Mei, Y. *J. Mater. Sci.* **2024,** *59,* 12129–12153. doi:10.1007/s10853-024-09850-8
68. Cao, W.; Nie, J.; Cao, Y.; Gao, C.; Wang, M.; Wang, W.; Lu, X.; Ma, X.; Zhong, P. *Chem. Eng. J.* **2024,** *496,* 154097. doi:10.1016/j.cej.2024.154097
69. Kim, B. S. Y.; Ngo, T. D.; Hassan, Y.; Chae, S. H.; Yoon, S.-G.; Choi, M. S. *Adv. Sci.* **2024,** *11,* 2407175. doi:10.1002/advs.202407175
70. Wang, C.; Long, Y.; Deng, Y.; Han, Y.; Tishkevich, D.; Ha, M. N.; Weng, Q. *BMEMat* **2024,** *2,* e12068. doi:10.1002/bmm2.12068
71. Reynoso, A. J.; Djakovitch, L.; Loridant, S.; Epicier, T.; Perret, N. *ChemCatChem* **2026,** *18,* e01587. doi:10.1002/cctc.202501587
72. Doroshina, N. V.; Streletskiy, O. A.; Zavidovskiy, I. A.; Tatmyshevskiy, M. K.; Tselikov, G. I.; Kapitanova, O. O.; Syuy, A. V.; Romanov, R.; Mishra, P.; Bobrovs, V.; Markeev, A. M.; Yakubovsky, D. I.; Veselova, I. A.; Arsenin, A. V.; Volkov, V. S.; Novikov, S. M. *Heliyon* **2024,** *10,* e27538. doi:10.1016/j.heliyon.2024.e27538
73. Li, C.; Lu, Y.; Yan, J.; Yu, W.; Zhao, R.; Du, S.; Niu, K. *R. Soc. Open Sci.* **2021,** *8,* 202309. doi:10.1098/rsos.202309
74. Carreira-Barral, I.; Díez-Hernández, J.; Igos, E.; Saidani, M.; Ding, T.; Ramos da Silva, T.; Monteiro, H.; Stingl, A.; Farias, P. M. A.; Cardozo, O.; Ibáñez, J.; García-Moral, A.; Tamayo-Ramos, J. A.; Rumbo, C.; Barros, R.; Martel-Martín, S. *Sustainable Prod. Consumption* **2025,** *55,* 353–372. doi:10.1016/j.spc.2025.03.003
75. Mukherjee, S. P.; Gliga, A. R.; Lazzaretto, B.; Brandner, B.; Fielden, M.; Vogt, C.; Newman, L.; Rodrigues, A. F.; Shao, W.; Fournier, P. M.; Toprak, M. S.; Star, A.; Kostarelos, K.; Bhattacharya, K.; Fadeel, B. *Nanoscale* **2018,** *10,* 1180–1188. doi:10.1039/c7nr03552g
76. Tian, B.; Tian, B.; Smith, B.; Scott, M. C.; Lei, Q.; Hua, R.; Tian, Y.; Liu, Y. *Proc. Natl. Acad. Sci. U. S. A.* **2018,** *115,* 4345–4350. doi:10.1073/pnas.1800069115
77. Zaed, M. A.; Han, T. K.; Rahman, S.; Panday, A. K.; Saleque, A. M. *Open Ceram.* **2024,** *17,* 100526. doi:10.1016/j.oceram.2023.100526
78. Han, M. *Natl. Sci. Rev.* **2025,** *12,* nwaf431. doi:10.1093/nsr/nwaf431
79. Zhang, X.; Pan, H.; Zheng, N.; Zhang, Y.; Lv, Y.; Wu, C.; Yu, J.; Wei, R.; Gao, T.; Yu, Y.; Yang, N.; Liu, W. *Cell Rep. Phys. Sci.* **2024,** *5,* 102124. doi:10.1016/j.xcrp.2024.102124
80. Fukamachi, S.; Solís-Fernández, P.; Kawahara, K.; Tanaka, D.; Otake, T.; Lin, Y.-C.; Suenaga, K.; Ago, H. *Nat. Electron.* **2023,** *6,* 126–136. doi:10.1038/s41928-022-00911-x
81. Vlassiouk, I.; Smirnov, S.; Puretzky, A.; Olunloyo, O.; Geohegan, D. B.; Dyck, O.; Lupini, A. R.; Unocic, R. R.; Meyer, H. M., III; Xiao, K.; Briggs, D.; Lavrik, N.; Keum, J.; Cakmak, E.; Harris, S. B.; Checa, M.; Collins, L.; Lasseter, J.; Emery, R.; Rayle, J.; Rack, P. D.; Stehle, Y.; Chaturvedi, P.; Kidambi, P. R.; Gu, G.; Ivanov, I. *Adv. Mater. Interfaces* **2024,** *11,* 2300704. doi:10.1002/admi.202300704
82. Dey, S.; Mohanty, D. I.; Divya, N.; Bakshi, V.; Mohanty, A.; Rath, D.; Das, S.; Mondal, A.; Roy, S.; Sabui, R. *Intell. Pharm.* **2025,** *3,* 53–70. doi:10.1016/j.ipha.2024.08.004
83. Harishchandra, B. D.; Pappuswamy, M.; PU, A.; Shama, G.; Pragatheesh, A.; Arumugam, V. A.; Periyaswamy, T.; Sundaram, R. *Asian Pac. J. Cancer Biol.* **2020,** *5,* 201–210.
84. Eker, F.; Duman, H.; Akdaşçi, E.; Witkowska, A. M.; Bechelany, M.; Karav, S. *Nanomaterials* **2024,** *14,* 1618. doi:10.3390/nano14201618
85. Abdel-Motagaly, A. T.; El Rouby, W. M. A.; El-Dek, S. I.; El-Sherbiny, I. M.; Farghali, A. A. *Diamond Relat. Mater.* **2018,** *86,* 20–28. doi:10.1016/j.diamond.2018.04.006
86. Xiong, S.; Chen, X.; Liu, Y.; Fan, T.; Wang, Q.; Zhang, H.; Chen, T. *J. Innovative Opt. Health Sci.* **2020,** *13,* 2030008. doi:10.1142/s1793545820300086
87. Favron, A.; Gaufrès, E.; Fossard, F.; Phaneuf-L'Heureux, A.-L.; Tang, N. Y.-W.; Lévesque, P. L.; Loiseau, A.; Leonelli, R.; Francoeur, S.; Martel, R. *Nat. Mater.* **2015,** *14,* 826–832. doi:10.1038/nmat4299
88. Castellanos-Gomez, A.; Vicarelli, L.; Prada, E.; Island, J. O.; Narasimha-Acharya, K. L.; Blanter, S. I.; Groenendijk, D. J.; Buscema, M.; Steele, G. A.; Alvarez, J. V.; Zandbergen, H. W.; Palacios, J. J.; van der Zant, H. S. J. *2D Mater.* **2014,** *1,* 025001. doi:10.1088/2053-1583/1/2/025001
89. Yin, W.; Sun, S.; Yao, H.; Li, W.; Cui, Y.; Peng, C. *ACS Biomater. Sci. Eng.* **2025,** *11,* 1317–1337. doi:10.1021/acsbiomaterials.4c02263
90. Zhang, H.; Shan, C.; Wu, K.; Pang, M.; Kong, Z.; Ye, J.; Li, W.; Yu, L.; Wang, Z.; Pak, Y. L.; An, J.; Gao, X.; Song, J. *ChemPlusChem* **2025,** *90,* e202400552. doi:10.1002/cplu.202400552

91. Liu, Y.; Chen, M.; Yang, S. *InfoMat* **2021,** *3,* 231–251. doi:10.1002/inf2.12171
92. Luo, M.; Fan, T.; Zhou, Y.; Zhang, H.; Mei, L. *Adv. Funct. Mater.* **2019,** *29,* 1808306. doi:10.1002/adfm.201808306
93. Sun, L.; Han, Y.; Zhao, Y.; Cui, J.; Bi, Z.; Liao, S.; Ma, Z.; Lou, F.; Xiao, C.; Feng, W.; Liu, J.; Cai, B.; Li, D. *Front. Pharmacol.* **2024,** *15,* 1396975. doi:10.3389/fphar.2024.1396975
94. Wu, J.; Xu, R.; Shao, M.; Zhao, L.; Xu, W.; Guo, Y. *ACS Appl. Nano Mater.* **2024,** *7,* 11022–11036. doi:10.1021/acsanm.4c00015
95. Würthner, F.; Saha-Möller, C. R.; Fimmel, B.; Ogi, S.; Leowanawat, P.; Schmidt, D. *Chem. Rev.* **2016,** *116,* 962–1052. doi:10.1021/acs.chemrev.5b00188
96. Jiang, Y.; Zheng, W.; Tran, K.; Kamilar, E.; Bariwal, J.; Ma, H.; Liang, H. *Nat. Commun.* **2022,** *13,* 197. doi:10.1038/s41467-021-27193-9
97. Punz, B.; Christ, C.; Waldl, A.; Li, S.; Liu, Y.; Johnson, L.; Auer, V.; Cardozo, O.; Farias, P. M. A.; Andrade, A. C. D. S.; Stingl, A.; Wang, G.; Li, Y.; Himly, M. *Environ. Sci.: Nano* **2025,** *12,* 1710–1739. doi:10.1039/d4en00798k
98. Ma, H.; Xue, M. *J. Mater. Chem. A* **2021,** *9,* 17569–17591. doi:10.1039/d1ta04134g
99. Dediu, V.; Ghitman, J.; Gradisteanu Pircalabioru, G.; Chan, K. H.; Iliescu, F. S.; Iliescu, C. *Int. J. Mol. Sci.* **2023,** *24,* 9375. doi:10.3390/ijms24119375
100. Wu, N.; Wang, X.; Das, C. M.; Ma, M.; Qiao, N.; Fan, T.; Zhang, H.; Xu, G.; Yong, K.-T. *Environ. Sci.: Nano* **2021,** *8,* 3452–3477. doi:10.1039/d1en00273b
101. Hoseini-Ghahfarokhi, M.; Mirkiani, S.; Mozaffari, N.; Abdolahi Sadatlu, M. A.; Ghasemi, A.; Abbaspour, S.; Akbarian, M.; Farjadian, F.; Karimi, M. *Int. J. Nanomed.* **2020,** *15,* 9469–9496. doi:10.2147/ijn.s265876
102. Zhang, B.; Wei, P.; Zhou, Z.; Wei, T. *Adv. Drug Delivery Rev.* **2016,** *105,* 145–162. doi:10.1016/j.addr.2016.08.009
103. Xu, S.; Chang, L.; Hu, Y.; Zhao, X.; Huang, S.; Chen, Z.; Ren, X.; Mei, X. *J. Nanobiotechnol.* **2021,** *19,* 362. doi:10.1186/s12951-021-01106-w
104. Damiri, F.; Rahman, M. H.; Zehravi, M.; Awaji, A. A.; Nasrullah, M. Z.; Gad, H. A.; Bani-Fwaz, M. Z.; Varma, R. S.; Germoush, M. O.; Al-malky, H. S.; Sayed, A. A.; Rojekar, S.; Abdel-Daim, M. M.; Berrada, M. *Materials* **2022,** *15,* 1666. doi:10.3390/ma15051666
105. Gaba, S.; Sahu, M.; Chauhan, N.; Jain, U. *Talanta Open* **2025,** *12,* 100498. doi:10.1016/j.talo.2025.100498
106. Manhas, S.; Khajuria, S.; Verma, M.; Ahmed, S.; Bhat, A. R.; Upadhye, V. J.; Kundan, S. *Sci. Rep.* **2026,** *16,* 3455. doi:10.1038/s41598-025-33484-8
107. Gungordu Er, S.; Edirisinghe, M.; Tabish, T. A. *Adv. Healthcare Mater.* **2023,** *12,* 2201523. doi:10.1002/adhm.202201523
108. Zare Mehrabadi, F.; Haddad, M. A.; Hosseini Motlagh, N. S.; Zarei Mahmoudabadi, M.; Sardari Zarchi, M.; Haghiralsadat, B. F. *Lasers Med. Sci.* **2025,** *40,* 50. doi:10.1007/s10103-025-04311-3
109. Zeng, G.; Chen, Y. *Acta Biomater.* **2020,** *118,* 1–17. doi:10.1016/j.actbio.2020.10.004
110. Choi, J. R.; Yong, K. W.; Choi, J. Y.; Nilghaz, A.; Lin, Y.; Xu, J.; Lu, X. *Theranostics* **2018,** *8,* 1005–1026. doi:10.7150/thno.22573
111. Li, H.-x.; Zhao, K.-c.; Jiang, J.-j.; Zhu, Q.-s. *J. Biol. Eng.* **2023,** *17,* 8. doi:10.1186/s13036-023-00328-w
112. Ouyang, J.; Ji, X.; Zhang, X.; Feng, C.; Tang, Z.; Kong, N.; Xie, A.; Wang, J.; Sui, X.; Deng, L.; Liu, Y.; Kim, J. S.; Cao, Y.; Tao, W. *Proc. Natl. Acad. Sci. U. S. A.* **2020,** *117,* 28667–28677. doi:10.1073/pnas.2016268117
113. Zhao, Y.; Chen, Z.; Shao, W.; Yang, S.; Cui, W.; Cai, Z.; Cheng, L.; Lin, R. *APL Bioeng.* **2023,** *7,* 016103. doi:10.1063/5.0121241
114. Zhang, C.; Wang, Y.; Ma, J.; Zhang, Q.; Wang, F.; Liu, X.; Xia, T. *Sci. Total Environ.* **2020,** *721,* 137740. doi:10.1016/j.scitotenv.2020.137740
115. Negut, I.; Grumezescu, V.; Grumezescu, A. M. *Molecules* **2018,** *23,* 2392. doi:10.3390/molecules23092392
116. Virgo, E. P.; Haidari, H.; Shaw, Z. L.; Huang, L. Z. Y.; Kennewell, T. L.; Smith, L.; Ahmed, T.; Bryant, S. J.; Howarth, G. S.; Walia, S.; Cowin, A. J.; Elbourne, A.; Kopecki, Z. *Adv. Ther. (Weinheim, Ger.)* **2023,** *6,* 2300235. doi:10.1002/adtp.202300235
117. Liu, L.; Wang, W.; Hong, W.; Jin, Y.; Wang, L.; Liu, S.; Wang, A.; Liu, X. *Front. Bioeng. Biotechnol.* **2022,** *9,* 826011. doi:10.3389/fbioe.2021.826011
118. Wang, H.; Yang, X.; Shao, W.; Chen, S.; Xie, J.; Zhang, X.; Wang, J.; Xie, Y. *J. Am. Chem. Soc.* **2015,** *137,* 11376–11382. doi:10.1021/jacs.5b06025
119. Huang, S.; Xu, S.; Hu, Y.; Zhao, X.; Chang, L.; Chen, Z.; Mei, X. *Acta Biomater.* **2022,** *137,* 199–217. doi:10.1016/j.actbio.2021.10.008
120. Bai, X.; Wang, R.; Hu, X.; Dai, Q.; Guo, J.; Cao, T.; Du, W.; Cheng, Y.; Xia, S.; Wang, D.; Yang, L.; Teng, L.; Chen, D.; Liu, Y. *ACS Nano* **2024,** *18,* 3553–3574. doi:10.1021/acsnano.3c11177
121. Ding, X.; Yu, Y.; Fan, L.; Li, W.; Bian, F.; Wang, J.; Zhao, Y. *Adv. Healthcare Mater.* **2024,** *13,* 2302588. doi:10.1002/adhm.202302588
122. Zhang, X.; Chen, G.; Liu, Y.; Sun, L.; Sun, L.; Zhao, Y. *ACS Nano* **2020,** *14,* 5901–5908. doi:10.1021/acsnano.0c01059
123. Cao, X.; Xu, D.; Lu, M.; Zhao, Y. *Chem. Eng. J.* **2025,** *520,* 166356. doi:10.1016/j.cej.2025.166356
124. Takhar, V.; Singh, S. *Environ. Sci.: Nano* **2025,** *12,* 2516–2550. doi:10.1039/d5en00049a
125. Davies, K. J. A. *IUBMB Life* **2000,** *50,* 279–289. doi:10.1080/713803728
126. Pope, L. D.; Kodakkat, S.; Elbourne, A.; Sherrell, P. C.; Tran, N.; Fox, K. *Molecules* **2025,** *30,* 2292. doi:10.3390/molecules30112292
127. Dong, H.; Wen, Y.; Lin, J.; Zhuang, X.; Xian, R.; Li, P.; Li, S. *J. Funct. Biomater.* **2023,** *14,* 284. doi:10.3390/jfb14050284
128. Yu, W.; Xu, J.; Chen, F.; Wang, Y.; Tang, S.; Geng, F.; Lv, J.; Qu, G.; Zhao, L.; Wang, Y. *Angew. Chem., Int. Ed.* **2022,** *61,* e202213595. doi:10.1002/anie.202213595
129. Seixas, A. F.; Quendera, A. P.; Sousa, J. P.; Silva, A. F. Q.; Arraiano, C. M.; Andrade, J. M. *Front. Genet.* **2022,** *12,* 821535. doi:10.3389/fgene.2021.821535
130. Jiang, L.; Luo, M.; Wang, J.; Ma, Z.; Zhang, C.; Zhang, M.; Zhang, Q.; Yang, H.; Li, L. *Nanoscale* **2024,** *16,* 12287–12308. doi:10.1039/d4nr02026j
131. Tan, L.; Li, J.; Liu, X.; Cui, Z.; Yang, X.; Yeung, K. W. K.; Pan, H.; Zheng, Y.; Wang, X.; Wu, S. *Small* **2018,** *14,* 1703197. doi:10.1002/smll.201703197
132. Circu, M. L.; Aw, T. Y. *Free Radical Biol. Med.* **2010,** *48,* 749–762. doi:10.1016/j.freeradbiomed.2009.12.022
133. Liu, T.; She, W.; Du, R.; Bao, Y.; Guo, Z.; Gao, Q.; Li, H.; Suo, P.; Liu, Y.; Liu, Y. *Mater. Today Bio* **2026,** *37,* 102862. doi:10.1016/j.mtbio.2026.102862

134. Shaw, Z. L.; Kuriakose, S.; Cheeseman, S.; Mayes, E. L. H.; Murali, A.; Oo, Z. Y.; Ahmed, T.; Tran, N.; Boyce, K.; Chapman, J.; McConville, C. F.; Crawford, R. J.; Taylor, P. D.; Christofferson, A. J.; Truong, V. K.; Spencer, M. J. S.; Elbourne, A.; Walia, S. *ACS Appl. Mater. Interfaces* **2021,** *13,* 17340–17352. doi:10.1021/acsami.1c01739
135. Liang, M.; Zhang, M.; Yu, S.; Wu, Q.; Ma, K.; Chen, Y.; Liu, X.; Li, C.; Wang, F. *Small* **2020,** *16,* 1905938. doi:10.1002/smll.201905938
136. Ruiz, A.; Martín, C.; Reina, G. *Nanoscale Adv.* **2021,** *3,* 4029–4036. doi:10.1039/d1na00203a
137. Li, C.; Xu, Q.; Xu, S.; Zhang, X.; Hou, X.; Wu, P. *RSC Adv.* **2017,** *7,* 16204–16209. doi:10.1039/c7ra01244f
138. Perreault, F.; de Faria, A. F.; Nejati, S.; Elimelech, M. *ACS Nano* **2015,** *9,* 7226–7236. doi:10.1021/acsnano.5b02067
139. Chowdhury, I.; Duch, M. C.; Mansukhani, N. D.; Hersam, M. C.; Bouchard, D. *Environ. Sci. Technol.* **2013,** *47,* 6288–6296. doi:10.1021/es400483k
140. Li, B.; Yang, J.; Huang, Q.; Zhang, Y.; Peng, C.; Zhang, Y.; He, Y.; Shi, J.; Li, W.; Hu, J.; Fan, C. *NPG Asia Mater.* **2013,** *5,* e44. doi:10.1038/am.2013.7
141. Yang, K.; Gong, H.; Shi, X.; Wan, J.; Zhang, Y.; Liu, Z. *Biomaterials* **2013,** *34,* 2787–2795. doi:10.1016/j.biomaterials.2013.01.001
142. Ye, T.; Li, Y.; Zhou, X.; Ye, Y.; Liu, X.; Xiong, W. *J. Hazard. Mater.* **2025,** *487,* 137207. doi:10.1016/j.jhazmat.2025.137207
143. Zhou, J.; Li, T.; Zhang, M.; Han, B.; Xia, T.; Ni, S.; Liu, Z.; Chen, Z.; Tian, X. *J. Nanobiotechnol.* **2023,** *21,* 330. doi:10.1186/s12951-023-02054-3
144. Liu, B.; Su, Y.; Wu, S.; Shen, J. *Photodiagn. Photodyn. Ther.* **2022,** *39,* 102905. doi:10.1016/j.pdpdt.2022.102905
145. Qi, W.; Zhang, R.; Wang, Z.; Du, H.; Zhao, Y.; Shi, B.; Wang, Y.; Wang, X.; Wang, P. *Pharmaceuticals* **2024,** *17,* 242. doi:10.3390/ph17020242
146. Aksoy, İ.; Küçükkeçeci, H.; Sevgi, F.; Metin, Ö.; Hatay Patir, I. *ACS Appl. Mater. Interfaces* **2020,** *12,* 26822–26831. doi:10.1021/acsami.0c02524
147. Su, X.; Chi, Y.; Liu, T.; Xun, H.; Wu, Y.; Liu, X.; Zheng, J.; Hu, F.; Han, S.; Duan, H.; Chai, J. *ACS Appl. Mater. Interfaces* **2024,** *16,* 43892–43906. doi:10.1021/acsami.4c06075
148. Guo, Z.; He, J.-X.; Mahadevegowda, S. H.; Kho, S. H.; Chan-Park, M. B.; Liu, X.-W. *Adv. Healthcare Mater.* **2020,** *9,* 2000265. doi:10.1002/adhm.202000265
149. Guo, T.; Zhuang, S.; Qiu, H.; Guo, Y.; Wang, L.; Jin, G.; Lin, W.; Huang, G.; Yang, H. *Part. Part. Syst. Charact.* **2020,** *37,* 2000169. doi:10.1002/ppsc.202000169
150. Kodakkat, S.; Mirihana, K. A.; Penman, R.; Kariuki, R.; Valliant, P. H. A.; Christofferson, A. J.; Bryant, G.; Bryant, S. J.; Walia, S.; Elbourne, A. *J. Colloid Interface Sci.* **2025,** *694,* 137686. doi:10.1016/j.jcis.2025.137686
151. Liu, W.; Zhang, Y.; Zhang, Y.; Dong, A. *Chem. – Eur. J.* **2020,** *26,* 2478–2485. doi:10.1002/chem.201905134
152. Phakatkar, A. H.; Firlar, E.; Alzate, L.; Song, B.; Narayanan, S.; Rojaee, R.; Foroozan, T.; Deivanayagam, R.; Banner, D. J.; Shahbazian-Yassar, R.; Shokuhfar, T. *Int. J. Nanomed.* **2020,** *15,* 3071–3085. doi:10.2147/ijn.s237816
153. Qu, G.; Xia, T.; Zhou, W.; Zhang, X.; Zhang, H.; Hu, L.; Shi, J.; Yu, X.-F.; Jiang, G. *Chem. Rev.* **2020,** *120,* 2288–2346. doi:10.1021/acs.chemrev.9b00445
154. Chen, W.; Ouyang, J.; Liu, H.; Chen, M.; Zeng, K.; Sheng, J.; Liu, Z.; Han, Y.; Wang, L.; Li, J.; Deng, L.; Liu, Y.-N.; Guo, S. *Adv. Mater. (Weinheim, Ger.)* **2017,** *29,* 1603864. doi:10.1002/adma.201603864
155. Deng, F.; Wu, P.; Qian, G.; Shuai, Y.; Zhang, L.; Peng, S.; Shuai, C.; Wang, G. *Nanotechnology* **2022,** *33,* 245708. doi:10.1088/1361-6528/ac5aee
156. Zhang, D.; Liu, H. M.; Shu, X.; Feng, J.; Yang, P.; Dong, P.; Xie, X.; Shi, Q. *J. Hazard. Mater.* **2020,** *393,* 122317. doi:10.1016/j.jhazmat.2020.122317
157. Yang, Y.; Sha, P.; Li, P.; Xu, Z.; Cui, Y.; Ban, X.; Wang, Z.; Wang, C.; Guo, Y.; Yu, Z.; Zhang, Z.; Ren, L. *Nano Lett.* **2025,** *25,* 12769–12778. doi:10.1021/acs.nanolett.5c03614
158. Wu, Q.; Wang, X.; Li, Z.; Yang, R.; Fan, Y.; Lyu, J.; Wang, J.; Wang, S.; Wei, Y.; Liang, Z.; Han, W.; Zhao, L.; Huang, D. *Colloids Surf., A* **2026,** *737,* 139834. doi:10.1016/j.colsurfa.2026.139834
159. Ma, T.; Zhai, X.; Zhang, M.; Jin, M.; Zhao, X.; Hou, W.; Zhang, D.; Du, Y. *J. Rare Earths* **2026,** in press. doi:10.1016/j.jre.2026.01.014
160. Liu, X.; Kang, Q.; Yang, C.; Shi, S.; Zhang, Y.; Xiao, L.; Zhu, W.; Liu, Y. *Biomacromolecules* **2026,** *27,* 783–794. doi:10.1021/acs.biomac.5c02053

License and Terms

This is an open access article licensed under the terms of the Beilstein-Institut Open Access License Agreement (https://www.beilstein-journals.org/bjnano/terms), which is identical to the Creative Commons Attribution 4.0 International License (https://creativecommons.org/licenses/by/4.0). The reuse of material under this license requires that the author(s), source and license are credited. Third-party material in this article could be subject to other licenses (typically indicated in the credit line), and in this case, users are required to obtain permission from the license holder to reuse the material.

The definitive version of this article is the electronic one which can be found at:
https://doi.org/10.3762/bjnano.17.116